Available online at www.sciencedirect.com
ScienceDirect
Journal of Solid State Chemistry 180 (2007) 670–678
JOURNAL OF SOLID STATE CHEMISTRY
www.elsevier.com/locate/jssc

Titanium vacancy defects in sol–gel prepared anatase

Ian.E. Grey*, Nicholas C. Wilson

CSIRO Minerals, Bayview Avenue, Clayton, Vic., 3169, Australia

Received 18 September 2006; received in revised form 20 November 2006; accepted 22 November 2006
Available online 1 December 2006

Abstract

Rietveld refinement of powder X-ray diffraction data for nanocrystalline anatase samples prepared by different sol–gel methods shows that the samples contain high concentrations ($\leqslant 20\%$) of titanium vacancies, the levels of which decrease with increasing crystallite size. Debye function modelling of anatase clusters with different well-defined sizes, shapes and stoichiometries confirmed that the titanium vacancy concentrations obtained from the Rietveld refinements are correct. However, the Debye modelling showed that for nanocrystals smaller than ~4 nm, the Rietveld modelling gives artificially high cell parameters. Density function theory calculations show that the titanium vacancies are stable defects when the vacancy sites are charge-balanced by incorporation of protons.

Keywords: Debye function modeling of nano-TiO_2; Debye function testing of Rietveld method for nano-TiO_2; DFT modeling of Ti vacancies in TiO_2

1. Introduction

The burgeoning literature on TiO_2 photocatalysts is strongly focused on the preparation and characterisation of nanocrystalline materials. Such materials have the high surface areas that are necessary for efficient light harvesting in photocatalytic applications. However, the low-temperature sol–gel syntheses that are generally used to prepare nanocrystalline materials can lead to the formation of high concentrations of defects, particularly at the surface, which can have a strong influence on the photocatalytic performance. An understanding of defect chemistry is thus essential in the development of efficient TiO_2-based photocatalysts and photoelectrodes [1].

Oxygen vacancies are by far the most thoroughly studied defects in sol–gel prepared TiO_2. They are considered to play an important role in extending the photoactivity of the TiO_2 into the visible region of the solar spectrum [2,3]. In comparison, titanium vacancies have received scant attention, and most studies concern their role in contributing to *p*-type conductivity of dense single-crystal or polycrystalline rutile at high temperatures [4]. Mizushima et al. [5] proposed the presence of titanium vacancies as native defects in oxidised metal-doped rutile to explain their photocurrent spectra results. In a recent study, Phattalung et al. [6] applied first principles quantum mechanical calculations to determine the formation energies of different native defects in anatase form TiO_2. The defects considered included oxygen vacancies and interstitials, and titanium vacancies and interstitials. Their results showed that titanium vacancies had the lowest formation energies under oxygen-rich growth conditions such as would prevail in sol–gel preparations.

Experimental evidence for titanium vacancies in sol–gel prepared TiO_2 was obtained by Bokhimi et al. [7] and by Wang et al. [8] from Rietveld refinement of powder X-ray diffraction data. It was proposed that the titanium vacancies compensated for hydroxyl ion incorporation into the structure [8]. In heated anatase samples the titanium vacancy concentration was observed to decrease with increasing crystallite size [7]. We have recently confirmed these results from Rietveld refinements on nanocrystalline anatase samples prepared using different sol–gel methods [9].

A possible criticism of the use of the Rietveld method to quantify the concentration of titanium vacancies in nanocrystalline samples is that it is based on the assumption of a 3-D periodic lattice. Such 3-D periodicity is of a limited extent for nanocrystals as the size decreases below

*Corresponding author. Fax: +61 3 9562 8919.
E-mail address: ian.grey@csiro.au (I.E. Grey).

0022-4596/$ - see front matter © 2006 Elsevier Inc. All rights reserved.
doi:10.1016/j.jssc.2006.11.028

~10 nm and an increasingly important fraction of the atoms are located at the crystallite surface. Under these conditions it is possible that the apparent incomplete occupancy of the titanium sites obtained from the refinement is an artefact due to the inadequacy of the Bragg-diffraction-based method to model the diffraction from the nanoparticles.

In this study we have used the Debye function [10] to check the validity of using the Rietveld method for nanocrystalline anatase samples. The Debye function gives an exact reproduction of the intensity scattered from an assemblage of randomly oriented particles. We calculated the Debye function scattering for anatase clusters of well-defined shapes, sizes and stoichiometry. The calculated diffraction patterns were then used as experimental input data in Rietveld refinements to check the limitations of the latter in reproducing the known particle characteristics, including the concentrations of titanium vacancies. The diffraction pattern modelling was complemented with quantum mechanical calculations on anatase containing titanium vacancies to establish the defect formation energies and to quantify the influence of hydroxyl ions on the stabilisation of the defects.

2. Experimental section

Nanocrystalline anatase samples were prepared using three different procedures reported in the literature:

(1) Controlled hydrolysis of titanium isopropoxide followed by aging at 80 °C [11].
(2) Neutralisation at 0 °C of a solution of $TiCl_4$ in dilute HCl with NH_4OH [12].
(3) Evaporation of a solution of tetrabutyl titanate and thiourea in ethanol [13].

Syntheses (1) and (2) gave nanocrystalline anatase with minor brookite as a second phase, whereas the product from synthesis (3) was amorphous and had to be heated to temperatures above 300 °C to crystallise anatase. The as-prepared samples were split into sub-samples which were heated in air for 1 h at temperatures in the range 100–600 °C. Selected sub-samples were also re-dispersed in water and heated hydrothermally in sealed Teflon-lined containers at 200 °C.

Thermal analyses were conducted in the temperature range 20–900 °C using a Setaram Simultaneous TGA/DTA instrument model 92. Sample weights of typically 50 mg were contained in platinum crucibles and heated in high-purity helium at a heating rate of 10 °C/min. The evolved gases were analysed using a Balzers Thermostar QS422 mass spectrometer.

Rietveld X-ray diffraction (XRD) intensity data sets were collected using a Philips 1050 goniometer fitted with a long fine-focus copper tube operated at 40 kV and 40 mA. The diffractometer was configured with a 1° diverging slit, 0.3 mm receiving slit, Soller slits and a diffracted beam graphite monochromator. The data sets were collected in step-scan mode over the 2θ range 10–140°, using a step interval of 0.025° and a counting time of 3 s per step.

Rietveld refinements were conducted using CSRIET, a GUI-version of the Rietveld program SR5, modelled on the DBW-type program [14], and further developed by Hill and Howard [15]. For consistency, the same refinement procedure was used for all samples. The profile parameters included the scale factor, a zero-shift parameter, a four-term polynomial for the background (zero to third-order coefficients), two half-width parameters (V and W in the Cagliotti expression [16]), a single pseudo-Voigt shape parameter and the cell parameters. The structural parameters that were refined included the z coordinate for oxygen (the only variable atomic coordinate in anatase), the site occupation factor for titanium and the isotropic temperature factors for titanium and oxygen. The latter were constrained to be equal to minimise the effects of any correlations with the titanium site occupancy and the scale factor. In samples where brookite was identified in the XRD pattern, it was included as a second phase and its scale factor and half-width parameters were refined. Scattering curves for Ti^{2+} and O^{2-} were employed, as test runs showed that use of the half-ionised scattering curve for titanium gave the correct (full occupation) refined site occupancy for titanium in well-crystallised anatase (Aldrich AR reagent with a crystallite size of ~90 nm).

Structural models for the Debye function analysis were obtained by excising clusters of different sizes and shapes from the 3-D lattice for anatase using the crystal and molecular structure visualisation program Diamond (http://www.crystalimpact.com). Care was taken to ensure that the clusters retained the TiO_2 stoichiometry. The Debye scattering from the different clusters was calculated using the DISCUS program [17] in the DIFFUSE program package (http://www.uni-wuerzburg.de/mineralogie/crystal/discus). In the Rietveld fitting of the Debye-function-generated powder diffraction patterns, a similar refinement procedure was used as for the refinement of the experimental patterns for the nanocrystalline samples. However, only two parameters (zero and first order) were used in the fitting of the background, and the temperature factor was kept constant for all refinements ($B = 0.05$ Å^2).

Spin-polarised quantum mechanical calculations were based on the density functional theory (DFT) approximation and were implemented using the VASP code [18]. A planewave cutoff energy of 396 eV was used and the **k**-space integrations were performed using a Monkhorst-Pack [19] sampling scheme with a $7 \times 7 \times 7$ **k**-point mesh. A $2 \times 2 \times 1$ anatase supercell was used for the modelling of titanium vacancies. The calculations involved relaxing the structure using a conjugate-gradients scheme to minimise the forces on all atoms. The procedure for relaxing the defect structures was to first relax the hydrogen atoms with all other atom and cell parameters fixed, then allow all atom parameters to relax while the cell parameters remained fixed, and finally allowing all parameters

to relax. Defect energies were calculated from: $E_{defect} = E_{tot} - E_{host} + n_{Ti}\mu_{Ti} - n_H\mu_H$ where E_{tot} and E_{host} are the total energies of the defect supercell and the host supercell, n_{Ti} and n_H are the number of Ti atoms removed and the number of hydrogen atoms added and μ_{Ti} and μ_H are the chemical potentials of titanium and hydrogen in their respective reservoirs, TiO_2 and H_2O, respectively.

3. Results

3.1. Thermal analysis results

Thermal analysis results for the product from synthesis procedure #2 are shown in Fig. 1. Similar results were obtained for other samples. The differential thermogravimetric curve shows a relatively sharp peak centred at a temperature of 110 °C, and a broad peak extending from 150 to 400 °C. The latter shows small subsidiary peaks superimposed on the broad peak at temperatures of ~220 and 320 °C. The weight losses above and below 150 °C were 5.5 and 11.7 wt%, respectively. The differential thermal analysis trace in Fig. 1 shows broad, shallow endotherms corresponding to the main weight loss peaks. Analysis of the evolved gases by mass spectrometry showed that the dominant gaseous product (~90%) was water vapour. The subsidiary weight loss peaks at 220 and 320 °C correspond to evolution of N_2O and NO_2 respectively, from decomposition of nitrate ion. HNO_3 was used as a peptising agent in synthesis #2.

3.2. Rietveld refinements on nanocrystalline anatase samples

An unusual feature of the crystallography of nanocrystalline anatase is the anisotropic change in the unit cell parameters with change in crystallite size. Our results confirm those reported recently by Li et al. [20] that the *c* parameter increases whereas the *a* parameter decreases in nanocrystalline anatase heated at successively higher temperatures. Li et al.'s study was conducted on samples prepared by hydrolysis of tetrabutyl titanate in anhydrous ethanol. Our results for anatase prepared by synthesis #2 are presented in Fig. 2. The abscissa axis shows both the temperature at which the sample was heated and the corresponding crystallite size obtained from the XRD peak broadening using the Scherrer equation. The *c* parameter increases almost linearly with increasing crystallite size whereas the *a* parameter decreases sharply with initial increase in crystallite size then flattens. As a result of these changes the cell volume initially decreases by 0.4% as the heating temperature is increased to 400 °C, and then increases by 0.3% with further increase in temperature to 600 °C. Possible origins of the anisotropic cell parameter changes will be presented in the Discussion section.

The anatase samples prepared by the three different preparative methods showed similar rates of increase of the *c* cell parameters with increasing crystallite size. However the absolute magnitudes of the cell parameters differed significantly for the three sample types. This is illustrated in Fig. 3. The plots of *c* parameter versus crystallite size have similar slopes for the three sample types, but the lines are offset by ~0.02 Å. Such systematic changes were not as well defined for the *a* parameter.

The refined titanium site occupation is plotted against crystallite size for the three different sample types in Fig. 4. A clear correlation is evident from the displayed trendline, with the site occupancy increasing with increasing crystallite size. The titanium sites are only 80% occupied for the as-prepared samples from synthesis methods 1 and 2. The heating conditions required to bring about full titanium site occupancy differs for the three types of samples. Those samples produced by thiourea neutralisation of titanium tetrabutoxide (synthesis #3) achieve full site occupancy when the crystallite size is ~8 nm whereas the other two types retain some titanium vacancies in crystallites greater than 10 nm.

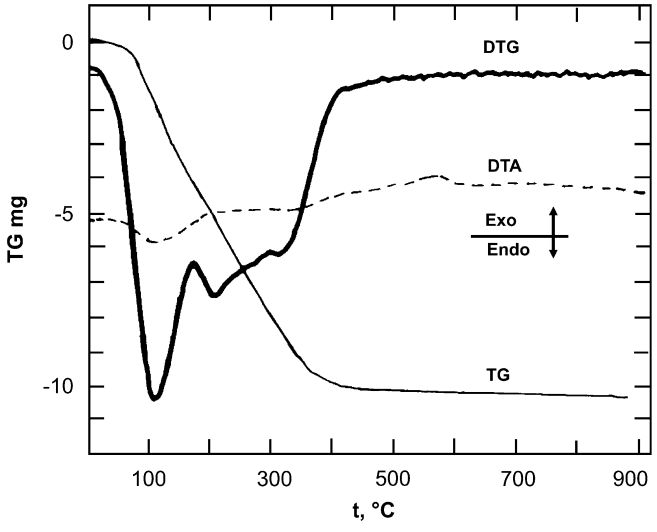

Fig. 1. Thermal analysis results for a sample prepared by synthesis method #2. The thin line represents the thermogravimetric (TG) weight loss, the thick line is the differential weight loss and the dashed line is the differential thermal analysis curve.

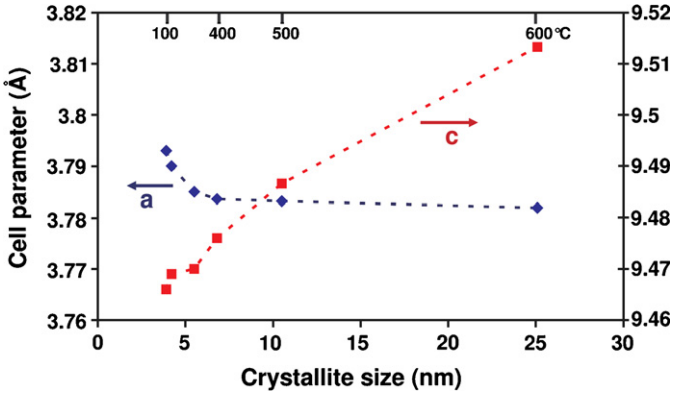

Fig. 2. Variation of unit cell parameters as a function of crystallite size for nanocrystalline anatase, prepared by synthesis method #2.

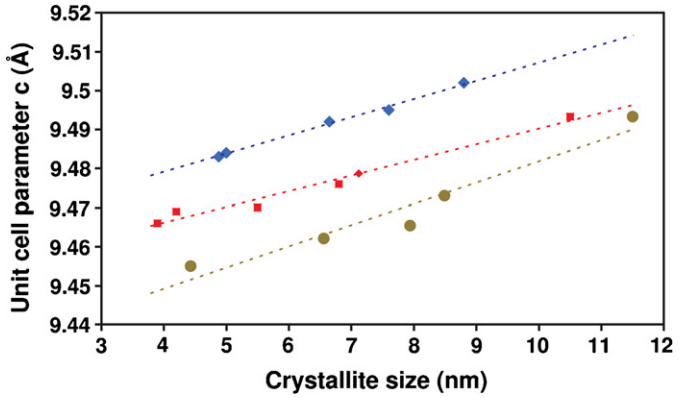

Fig. 3. Variation of *c*-axis parameter with crystallite size for nanocrystalline anatase. Circles, synthesis method 1; squares, synthesis method 2; diamonds, synthesis method 3. The small diamond is from synthesis method 3 after hydrothermal treatment at 200 °C.

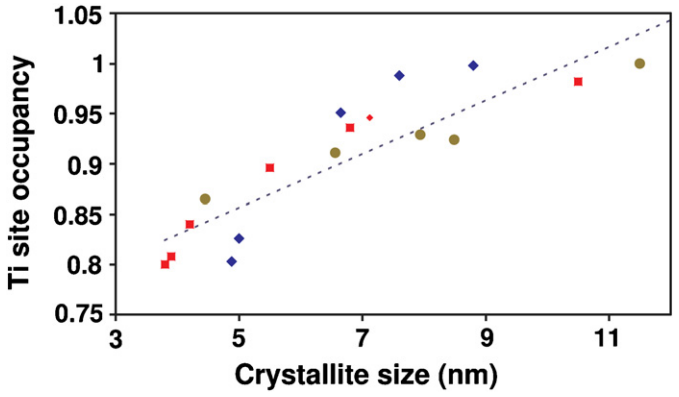

Fig. 4. Variation of titanium site occupancy for nanocrystalline anatase samples. Symbols correspond to different syntheses as given in Fig. 3.

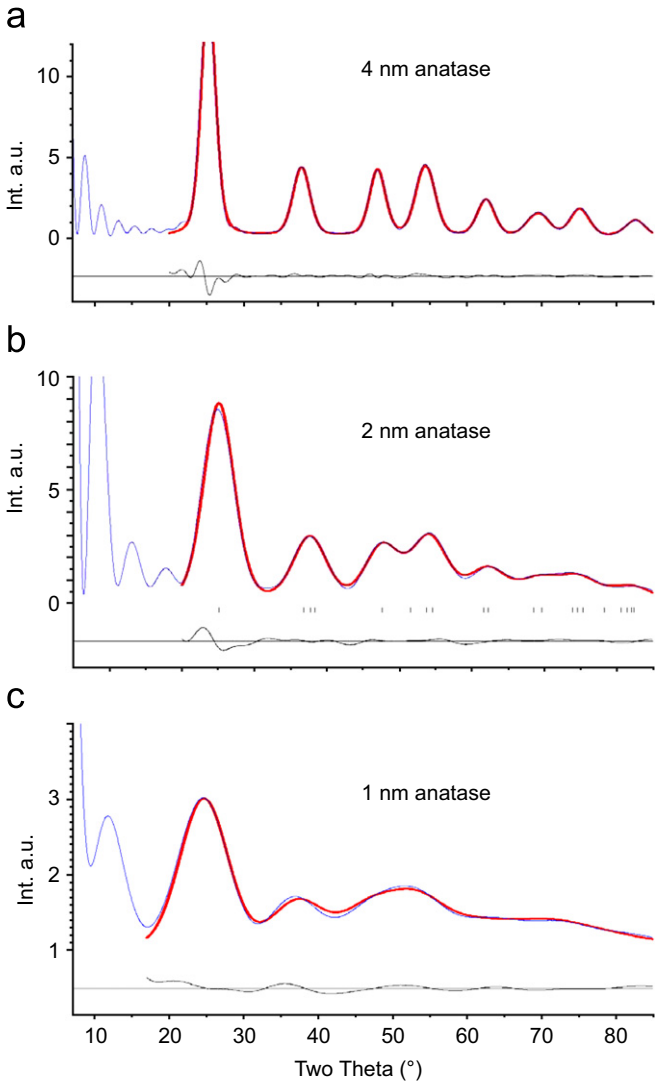

Fig. 5. Rietveld fit (solid curves) to Debye function-generated diffraction data for different size anatase spheres (fine dotted curves). Positions of Bragg reflections are shown below the diffractogram for the 2 nm sample. Difference plots shown below the diffractograms.

3.3. *Rietveld fitting of debye function scattering data*

Debye function scattering was generated for anatase spherical clusters of approximate diameters 1, 2 , 3 and 4 nm.The compositions of the clusters were $Ti_{36}O_{72}$, $Ti_{114}O_{228}$, $Ti_{403}O_{806}$ and $Ti_{976}O_{1952}$, respectively. The generated diffraction patterns for the 4, 2 and 1 nm clusters are shown by the fine dotted lines in Figs. 5(a)–(c). The Debye-calculated diffraction patterns are exact representations, within the kinematic approximation, of the diffraction from arrays of randomly oriented clusters with the same composition. The calculated scattering includes low angle scattering from the clusters, shown by the low-angle oscillations in Fig. 5. It is seen that the diffraction peaks are well resolved for the 4 nm cluster, and there is a progressive broadening and merging of the peaks and an increase in the background in the smaller clusters.

Rietveld fitting of the Debye-calculated scattering is shown by the solid lines in Fig. 5. Excellent fits were obtained for clusters $\geqslant$ 2 nm; the fit began to deteriorate only for the 1 nm cluster. Results from the Rietveld refinements are given in Table 1. The refined *a* and *c* lattice parameters are plotted as a function of the anatase cluster size in Fig. 6. For comparison the parameters for Aldrich AR anatase with crystallite size = 90 nm are displayed in Fig. 6. Within the associated standard deviations, the refined parameters for the 4 nm anatase cluster match those from the refinement of the Aldrich sample. However as the cluster size decreases below 4 nm, the diffraction peaks in the Debye-calculated patterns move progressively to lower angles and the resulting Rietveld-refined cell parameters increase markedly. The atomic periodicity in the different clusters was identical, so the peak shift is a feature of scattering from small clusters. The Rietveld analysis clearly gives incorrect cell parameters for anatase crystallite sizes below 4 nm.

Using the 4 nm cluster, different models for anatase containing titanium vacancies were generated. Approximately 5% and 15% of the titanium atoms were removed,

Table 1
Rietveld refinement of Debye function scattering for anatase clusters

Sample	R_{wp}	R_B	a (Å)	c (Å)	MCD (nm)	Ti SOF
1 nm, $Ti_{36}O_{72}$	7.7	2.4	3.888(1)	9.601(4)	1.1	1.121(6)
2 nm, $Ti_{114}O_{228}$	5.9	1.1	3.8168(4)	9.531(1)	1.6	1.023(4)
3 nm, $Ti_{403}O_{806}$	8.2	1.1	3.7935(3)	9.519(1)	2.6	0.985(5)
4 nm, $Ti_{976}O_{1952}$	8.0	1.0	3.7889(1)	9.517(1)	3.5	0.994(4)
4 nm—47* surface Ti	8.2	1.0	3.7885(2)	9.518(1)	3.4	0.976(4)
4 nm—161 surface Ti	9.8	1.8	3.7875(2)	9.523(1)	3.3	0.936(5)
4 nm—50 bulk Ti	8.3	1.1	3.7893(2)	9.516(1)	3.5	0.946(4)
4 nm—157 bulk Ti	9.4	1.8	3.7903(3)	9.515(1)	3.5	0.856(5)
$3.0 \times 3.0 \times 7.6$ nm $Ti_{2048}O_{4096}$	19.4	5.0	3.7907(3)	9.517(1)	3.7	0.856(8)

*Number of titanium atoms removed. R_{wp} = weighted profile agreement factor, R_B = Bragg agreement factor [15], MCD = mean crystallite dimension, SOF = site occupation factor.

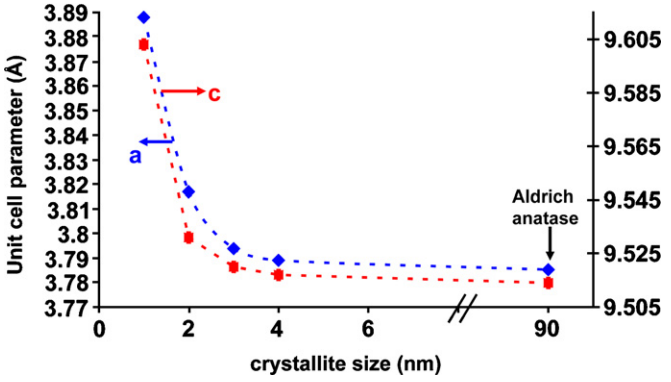

Fig. 6. Anatase lattice parameters from Rietveld refinement of Debye-scattering data for anatase spherical clusters, plotted versus cluster size.

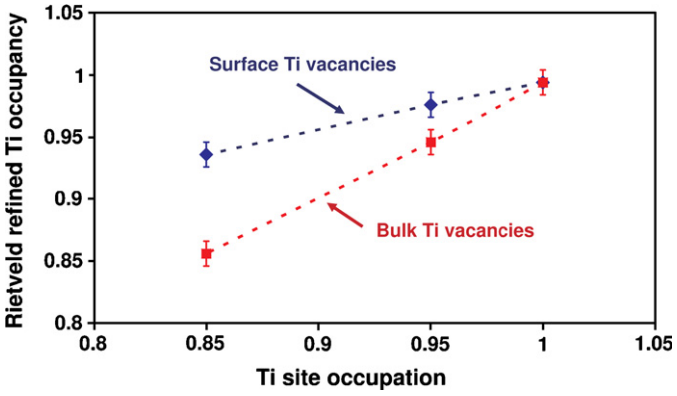

Fig. 7. Plot of Rietveld-refined titanium site occupancy versus actual occupancy in 4 nm anatase cluster, for titanium vacancies formed selectively at the surface (diamonds) and distributed randomly throughout the cluster (squares).

either from the surface of the cluster, or removed randomly throughout the bulk cluster. In each case the Debye-scattering was calculated and used as input to Rietveld refinements. The refinement results are given in Table 1. The refined titanium site occupancies are plotted versus the actual site occupancies in Fig. 7. For the models in which the titanium atoms were removed randomly throughout the bulk sample, the Rietveld refinement reproduces exactly the titanium site occupancy whereas for the models in which the titanium atoms were removed selectively from the surface, the Rietveld refinement strongly underestimates the fraction of titanium removed. From Table 1 it is seen that for the latter case, the refinement gives an apparently smaller mean crystallite dimension (MCD).

A few of the synthesised anatase samples showed preferential growth parallel to the c-axis, which was manifested as sharpened (00ℓ) reflections in the XRD pattern. Debye-modelling was used to check the effect of such anisotropic crystallite shapes on the Rietveld-derived structure parameters. An anatase cluster model was constructed with dimensions 3.0, 3.0 and 7.6 nm along the crystallographic axes. The Debye scattering from this model is shown in Fig. 8, together with the Rietveld fit to the data. The Rietveld program used did not have a capability for modelling anisotropic peak shapes and it is seen from Fig. 8 that the reflections with high ℓ values are poorly fitted. The Reitveld results for this model are given in Table 1. In attempting to reduce the weighted profile R factor the Rietveld refinement has resulted in an artificially low value for the titanium site occupancy (the occupancy should be 1). Care was subsequently taken, in the refinement of the diffraction data for the nanocrystalline anatase samples, to avoid samples that displayed peak anisotropy.

3.4. Quantum mechanical modelling results

Relaxation of an anatase defect model containing a single titanium vacancy in a $2 \times 2 \times 1$ cell gave a defect energy of 6.2 eV. This was calculated assuming the chemical reservoirs for Ti and O are bulk TiO_2 and gaseous oxygen in equilibrium, so that $\mu_{Ti} = \mu_{TiO_2} - 2\mu O$ and $\mu O = 1/2\mu O_2$ [21]. The high positive defect energy means that the concentration of such acceptor states will be

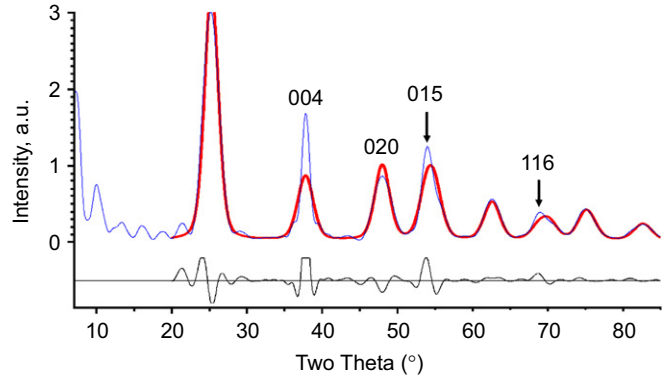

Fig. 8. Debye-scattering for a $3.0 \times 3.0 \times 7.6$ nm anatase cluster (fine dotted curve) with Rietveld refined fit (solid curve). Black line is the difference plot.

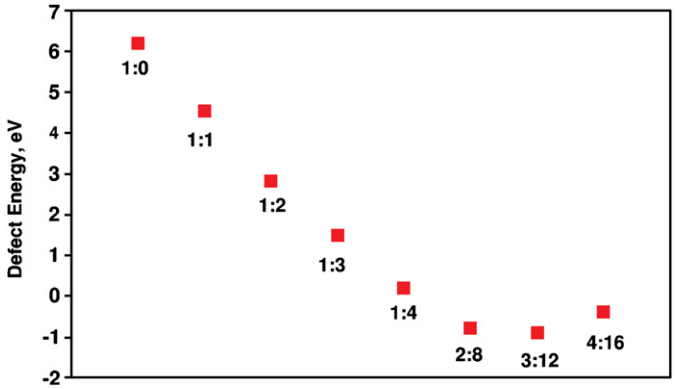

Fig. 9. Defect energies per defect for titanium vacancies in anatase, charge balanced with protons. The number of titanium vacancies and protons per $2 \times 2 \times 1$ anatase cell are shown by the pairs of numbers Ti:H.

extremely low. In sol–gel-prepared anatase samples, charge balance of titanium vacancies is most likely to be achieved by incorporation of hydroxide ions at the anion sites [8]. We checked this possibility using the DFT modelling and found that the incorporation of protons at the oxygen sites surrounding the titanium vacancy conferred stability on the defect.

The results of the defect energy calculations for different numbers of protons per vacancy and for different numbers of titanium vacancies, charge balanced with four protons, are plotted in Fig. 9. With four protons incorporated at the vacancy site the defect formation energy is lowered to 0.21 eV. The results in Fig. 9 indicate that when the titanium vacancy sites are fully charge-balanced by protons, $n\mathrm{Ti}^{4+} \leftrightarrow 4n\mathrm{H}^{+}$, the minimum energy is achieved at close to $n = 3$ titanium vacancies per 16 Ti atoms in the $2 \times 2 \times 1$ anatase cell. This corresponds to a defect anatase composition of $\mathrm{Ti}_{0.81}\square_{0.19}\mathrm{O}_{1.24}(\mathrm{OH})_{0.76}$, where $\square$ = vacancy, which matches closely with the vacancy concentration value of 0.2 (3.2 vacancies per 16 Ti atoms) obtained from Rietveld refinement of XRD data for the as-prepared sol–gel anatase samples as shown in Fig. 4.

4. Discussion

The presence of high concentrations of titanium vacancies in sol–gel prepared anatase samples was previously reported from Rietveld refinement of nanocrystalline samples [7], and has been confirmed in our own refinements [9]. A doubt remained however that such Rietveld-derived results may have been inaccurate, or even artefacts, of attempting to refine diffraction data from nanocrystals using Bragg-based methodology. To check this possibility we used the Debye function to calculate the powder diffraction patterns from arrays of randomly oriented anatase clusters of well-defined size, shape and stoichiometry and then used the calculated diffraction data as input data to Rietveld refinements. The approach showed that non-Bragg behaviour occurred when the cluster size was decreased below 4 nm. The progressive shift to lower angles of the peaks in the scattering pattern with decreasing cluster size was fitted using the Rietveld method by an artificial increase in the unit cell parameters. This result suggests that caution should be exercised in interpreting reported nanocrystal lattice parameter changes in terms of quantum size effects when the parameters have been obtained by classical Bragg-type fitting of the diffraction data.

In contrast with the cell parameter effects, the Debye function analysis confirmed that the Rietveld refinements accurately reproduce the correct concentrations of titanium vacancies in nanocrystalline anatase when the vacancies are distributed throughout the sample and not concentrated at the surface. The titanium vacancy concentrations shown in Fig. 4 that were obtained from Rietveld refinement of powder XRD data for sol–gel prepared samples can then be accepted with some degree of confidence. Quantum mechanical modelling showed that such titanium vacancies are stabilised in anatase by the incorporation of protons at the vacancy sites. Such charge-coupled cation vacancy/proton defects are well known in a number of other chemical systems, including γ-$\mathrm{MnO_2}$ ($\mathrm{Mn}^{4+} \leftrightarrow 4\,\mathrm{H}^{+}$) [22,23], hydrogarnets ($\mathrm{Si}^{4+} \leftrightarrow 4\,\mathrm{H}^{+}$) [24], hydrohematite ($\mathrm{Fe}^{3+} \leftrightarrow 3\,\mathrm{H}^{+}$) [25] and hydroxylian pseudorutile ($\mathrm{Fe}^{3+} \leftrightarrow 3\,\mathrm{H}^{+}$) [26]. The defects in γ-$\mathrm{MnO_2}$ have become known as Ruetschi defects after the person who first described them [22].

The model of titanium vacancies with charge-compensating hydroxyl ions in nanocrystalline anatase is supported by the thermal analysis data. Such data is shown for a freshly prepared sample from synthesis method #2 in Fig. 1. Rietveld refinement on this sample gave 20% titanium vacancies and the corresponding composition based on $\mathrm{Ti}^{4+} \leftrightarrow 4\,\mathrm{H}^{+}$ defects is $\mathrm{Ti}_{0.8}\square_{0.2}\mathrm{O}_{1.2}(\mathrm{OH})_{0.8}$. Loss of the hydroxyl ions as water on heating of this composition gives a calculated weight loss of 10.1%. Following Ruetschi [22], we assign the broad peak in the thermogravimetric curve above 150 °C to loss of structural water (hydroxyls). The total measured weight loss above 150 °C from Fig. 1 is 11.7%. Mass spectroscopy

measurements showed that about a tenth of this weight loss was due to evolution of NO_x species from the surface-adsorbed peptising agent, giving ~10.5 wt% of structural water, consistent with the model.

From thermal analysis studies on γ-MnO_2, Ruetschi and Giavanoli [23] concluded that the activation energy for structural water removal was determined by the activation energy of cation (vacancy) diffusion. On heating, the cation vacancies anneal out and the lower the cation vacancy fraction, the higher is the activation energy. Higher temperatures are thus needed to anneal out vacancies in samples with lower vacancy contents. This interpretation appears to apply also to the nano-anatase samples studied here. In Fig. 4, the as-prepared sample that has the lowest vacancy content (synthesis #3—filled circles) requires the highest temperature to completely anneal out the vacancies (as reflected in the lowest slope of the plot of titanium vacancy concentration vs crystallite size).

The nanocrystalline anatase samples that were prepared in this study all had mean crystallite dimensions greater than 4 nm and so the Rietveld-derived lattice parameters should not be affected by the non-Bragg behaviour shown in Fig. 6. The observed anisotropic cell parameter changes with change of crystallite size shown in Fig. 2 are characteristic of nanocrystalline anatase [8,9,20] and it is interesting to consider possible controlling influences. Stoneham [27] has described how the change in X-ray determined cell parameters of microcrystals with changing crystallite size can be related to the surface tension. It should be possible to quantify this effect from quantum mechanical calculations of the surface atomic relaxations at different bounding surfaces. However, the calculation is complicated by the nature of different adsorbing species on the surface. The displacements of the plots shown in Fig. 3 of c parameter vs. crystallite size for samples obtained from three different preparations is most likely a reflection of the different surface relaxations due to different surface adsorbates. This lends support to the Stoneham [27] model as a contributor to the observed cell parameter changes with crystallite size in nano-anatase.

An alternative explanation for the observed cell parameter changes in sol–gel prepared nano-anatase is based on the influence of titanium vacancies [9]. Of the different TiO_2 polymorphs (rutile, brookite, anatase, *hp*-TiO_2(high pressure form)) anatase is unusual in having the highest condensation of octahedra (4 shared edges per octahedron) but the lowest density. Strong repulsion of the highly charged titanium cations across the shared edges is accommodated by shortening of the 4 shared edges and a corresponding lengthening of the 4 unshared edges, leading to strongly elongated octahedra in the direction of the c-axis and a shortening of the distances normal to the c-axis.

The distortion of the octahedra in anatase is illustrated in Fig. 10, which shows equivalent views of anatase and *hp*-TiO_2 [28] normal to the close-packed oxygen planes in both structures. The comparison is made with *hp*-TiO_2 because it has the same zig-zag chains of edge-shared octahedra as in anatase. However, the anion layers have hexagonal stacking in *hp*-TiO_2 and cubic stacking in anatase and so the inter-layer octahedral articulation is via corner-sharing in *hp*-TiO_2 and edge-sharing in anatase. It is interesting to note that in this perspective based on close-packed anion layers, the TiO_2 polymorph brookite has mixed cubic and hexagonal stacking of the layers, *chch*, and its structure can be described simply as a 1:1 intergrowth of anatase and *hp*-TiO_2.

Fig. 10 shows the marked elongation of the octahedra in anatase along the chain direction relative to the octahedra in *hp*-TiO_2. There are 4 equivalent such chain directions in anatase, corresponding to the four equivalent {112} close-packed planes and the mean of the four chain directions is the c-axis direction. Relative to *hp*-TiO_2 the periodicity along the chain direction in anatase is 0.55 Å longer but the separation between the chains is 0.15 Å shorter [9].

In sol–gel prepared anatase, the presence of titanium vacancies results in a reduction in the extent of edge-sharing of the octahedra surrounding the vacancy. This relieves the strong Ti–Ti repulsions across the shared edges, and would thus be expected to result in more regular octahedra; that is, less elongated along the c direction with

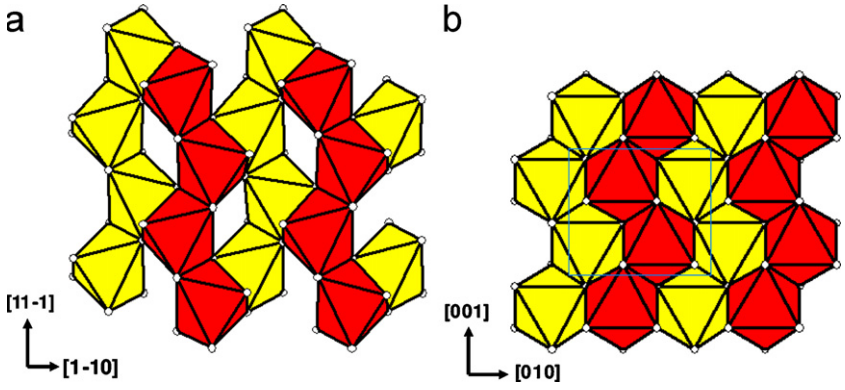

Fig. 10. Polyhedral representation of pairs of close-packed octahedral layers in (a) anatase and (b) *hp*-TiO_2. The close-packed layers are cubic-stacked in anatase and parallel to {112} while they are hexagonal-stacked in *hp*-TiO_2 and parallel to (100).

a compensating expansion normal to c. Thus sol–gel anatase should have a shortened c parameter and a lengthened a parameter, relative to well-crystallised anatase. The decrease in the titanium vacancy concentration with increasing crystallite size in heated nanocrystalline anatase samples then should result in the cell parameters changing towards the values in macro-crystalline anatase, as illustrated in Fig. 2.

The influence of titanium vacancies on the cell parameters is borne out by the results of the quantum mechanical (QM) relaxations. The unit cell parameters corresponding to relaxed $2 \times 2 \times 1$ supercells containing 0, 1, 2, 3 and 4 Ti vacancies are given in Table 2.

Table 2
Results from QM relaxations. $2 \times 2 \times 1$ anatase supercell ($Ti_{16}O_{32}$)

Number of titanium vacancies	$\langle a \rangle$[a] (Å)	c (Å)	Defect energy (eV)
0	7.60	9.64	n.a.
1	7.64	9.62	0.21
2	7.64	9.53	−0.78
3	7.66	9.48	−0.90
4	7.66	9.43	−0.38

[a] $\langle a \rangle$ is the average of a and b. These are equal in anatase but were allowed to vary independently in the QM relaxations.

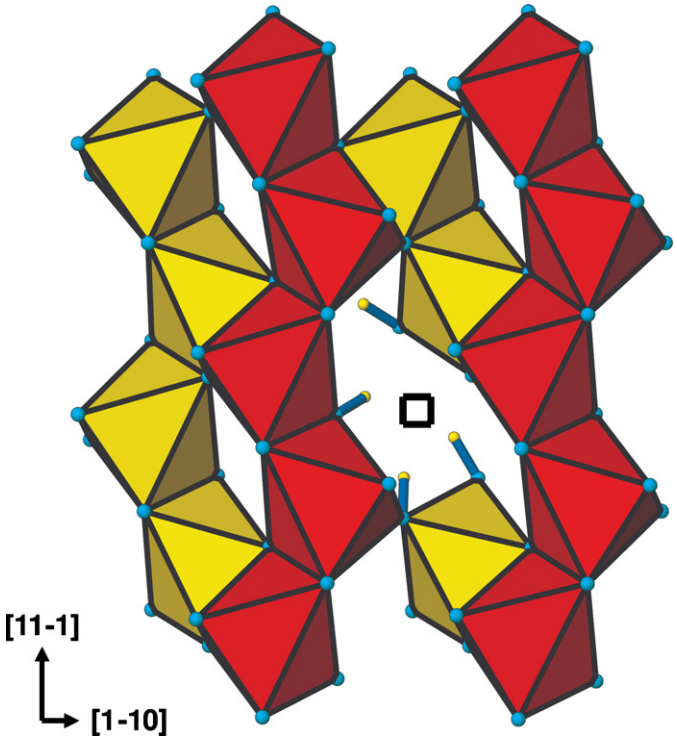

Fig. 11. Relaxed structure from DFT modelling of anatase containing one titanium vacancy and four protons per $2 \times 2 \times 1$ supercell. The perspective is the same as shown in Fig. 10(a). The four OH bonds are shown. The symbol □ represents the vacant titanium site.

The QM-derived parameters show the same trend as the experimental parameters in Table 1 of decreasing c and slightly increasing a with the increasing concentration of Ti vacancies that accompanies the decrease in crystallite size.

The QM calculations show that the titanium vacancies are stabilised by the incorporation of protons, forming hydroxyl anions around the vacancies. The DFT-relaxed model for anatase containing one titanium vacancy and four protons in the $2 \times 2 \times 1$ supercell is shown in Fig. 11. The four O–H distances obtained from the relaxation were in the range from 0.97 to 0.99 Å. Fig. 11 shows that only three of the four protons are located in the cavity formed by the titanium vacancy, with the fourth proton directed towards an adjacent channel. A similar location of Ruetschi-protons in channels was obtained in DFT calculations on Mn-deficient MnO_2 by Balachandran et al. [29]. We are currently extending the quantum mechanical calculations to the study of incorporation of dopant atoms C, B and N at vacant titanium sites in anatase and rutile. The preliminary results indicate that the three dopant atoms form stable defects in partially hydroxylated titanium vacancy sites.

5. Conclusions

Application of Debye function modelling to nanocrystalline anatase has shown that the use of powder XRD profile refinement procedures on such materials can lead to erroneous unit cell parameters for small crystallite sizes. In the case of anatase, the Rietveld-refined a and c cell parameters both increase markedly with decreasing crystallite size below 4 nm, even though identical atomic periodicities were used for the different-sized clusters. The Debye modelling also illustrates the shortcomings of the profile refinement method in refining data collected on nanocrystals with anisotropic shapes. If the refinement method does not have the capability for anisotropic peak width refinement, then unreasonable results for other refined parameters can result from the attempt to decrease the weighted profile agreement factor.

The Debye function modelling showed that for nanocrystals of uniform dimensions, the Rietveld-refined titanium site occupancies reproduces the correct concentrations of titanium vacancies, provided that the vacancies are uniformly distributed throughout the nanocrystals. For samples in which the titanium vacancies are concentrated at the surface, the Rietveld method greatly under-estimates the vacancy concentration. DFT quantum mechanical calculations showed that the titanium vacancies in anatase are stabilised by the incorporation of protons, forming hydroxyl ions around the vacant sites. For complete charge balance of the vacant sites, $n\mathrm{Ti}^{4+} \leftrightarrow 4n\mathrm{H}^{+}$, the DFT calculations give a minimum formation energy per defect at a defect anatase composition of $\sim \mathrm{Ti}_{0.81}\square_{0.19}\mathrm{O}_{1.24}(\mathrm{OH})_{0.76}$, $\square$ = vacancy.

Acknowledgments

We thank Christina Li for preparation of the anatase samples, Malisja de Vries for collecting XRD data on some of the samples, Terry Hall for the thermal analyses and Salvy Russo for discussion of the quantum mechanical modelling results. Thanks to the CSIRO Energy Transformed Flagship for support of the project and the Australian Partnership for Advanced Computing for the computational resources used in this project.

References

[1] J. Nowotny, C.C. Sorrell, T. Bak, L.R. Sheppard, Solar Energy 78 (2005) 593–602.
[2] I.N. Martyanov, S. Uma, S. Rodrigues, K.J. Klabunde, Chem. Commun. (2004) 2476–2477.
[3] I. Nakamura, N. Negishi, S. Kutsuna, T. Ihara, S. Sugihara, K. Takeuchi, J. Mol. Catal. A Chem. 161 (2000) 205–212.
[4] T. Bak, T. Burg, S.-J.L. Kang, J. Nowotny, M. Rekas, L. Sheppard, C.C. Sorrell, E.R. Vance, Y. Yoshida, M. Yamawaki, J. Phys. Chem. Solids 64 (2003) 1089–1095.
[5] K. Mizushima, M. Tanaka, A. Asai, S. Iida, J.B. Goodenough, J. Phys. Chem. Solids 40 (1979) 1129–1140.
[6] S.N. Phattalung, M.F. Smith, K. Kim, M.-H. Du, S.-H. Wei, S.B. Zhang, S. Limpijummong, Phys. Rev. B 73 (2006) 125205–125216.
[7] X. Bokhimi, A. Morales, O. Novaro, T. Lopez, E. Sanchez, R. Gomez, J. Mater. Res. 10 (1995) 2788–2796.
[8] J.A. Wang, R. Limas-Ballesteros, T. Lopez, A. Moreno, R. Gomez, O. Novaro, X. Bokhimi, J. Phys. Chem. B 105 (2001) 9692–9698.
[9] I. Grey, I. Madsen, P. Bordet, N. Wilson, C. Li, in: T. White, C. Ferraris, L. Yu, K. Halada, O. Umezawa (Eds.), Advances in Ecomaterials, vol. 1, Stallion Press, Singapore, 2005, pp. 35–42.
[10] P. Debye, Ann. Phys. 46 (1915) 809.
[11] W.W. So, S.B. Park, K.J. Kim, S.J. Moon, J. Colloid Interface Sci. 191 (1997) 398–406.
[12] S.K. Poznyak, A.I. Kokorin, A.I. Kulak, J. Electroanal. Chem. 442 (1998) 99–105.
[13] S. Yang, L. Gao, J. Am. Ceram. Soc. 87 (2004) 1803–1805.
[14] D.B. Wiles, R.A. Young, J. Appl. Crystallogr. 14 (1981) 149–151.
[15] R.J. Hill, C.J. Howard, Australian Atomic Energy Commission Report M112 (1986).
[16] G. Cagliotti, A. Paoletti, F.P. Ricci, Nucl. Instrum. 3 (1958) 223–228.
[17] T. Proffen, R.B. Neder, J. Appl. Crystallogr. 30 (1997) 171–175.
[18] G. Kresse, J. Furthmuller, Phys. Rev. B 54 (1996) 11169–11186.
[19] J.D. Pack, H.J. Monkhorst, Phys. Rev. B 13 (1976) 5188–5192.
[20] Y. Li, T.J. White, S.H. Lim, J. Solid State Chem. 177 (2004) 1372–1381.
[21] C.D. Valentin, G. Pacchioni A. Selloni, Chem. Mater. 17 (2005) 6656–6665.
[22] P. Ruetschi, J. Electrochem. Soc. 131 (1984) 2737–2744.
[23] P. Ruetschi, R. Giovanoli, J. Electrochem. Soc. 135 (1988) 2663–2669.
[24] G.A. Lager, T. Armbruster, J. Faber, Am. Mineral. 72 (1987) 756–765.
[25] E. Wolska, Z. Kristallogr. 154 (1981) 69–75.
[26] I.E. Grey, C. Li, Mineral. Mag. 67 (2003) 733–747.
[27] A.M. Stoneham, J. Phys. C: Solid State Phys. 10 (1977) 1175–1179.
[28] I.E. Grey, C. Li, I.C. Madsen, G. Braunshausen, Mater. Res. Bull. 23 (1988) 743–753.
[29] D. Balachandran, D. Morgan, G. Ceder, A. van der Walle, J. Solid State Chem. 173 (2003) 462–475.